Interface Effect on the Electronic Structure of Alkanethiol-Coated Platinum Nanoparticles

Weixia Tu, Kazuyuki Takai, Ken-ichi Fukui, Akira Miyazaki, and Toshiaki Enoki*

Department of Chemistry, Tokyo Institute of Technology, Tokyo 152-8551, Japan

Received: March 22, 2003; In Final Form: June 16, 2003

The structure and electronic properties are investigated for Pt nanoparticles coated with octadecanethiol self-assembled monolayer. The increase in the octadecanethiol/Pt ratio from 0 to full coverage reduces the average particle size from 2.2 to 0.9 nm. The temperature-independent spin susceptibility rises upon the increase in the particle size, quantum size effect being suggested to govern the magnetism. The low-temperature susceptibility shows a large Curie-type divergence, which cannot be explained simply by the even electron state of Pt. XPS spectra suggest an electron deficiency in the interior Pt nanoparticles, which is brought about by charge transfer from nanoparticle to coating thiol monolayer. The ESR line width and the *g*-value deviation increase as the octadecanethiol/Pt ratio is elevated, which are associated with the enhancement of spin−orbit interaction at the interface between the interior nanoparticle and coating thiol monolayer. This change at the interface works to make first spin−lattice relaxation centers in the carrier scattering process.

Introduction

Recently, metal nanoparticles have generated considerable interest in supramolecular chemistry and nanoscopic physics. They have properties distinguished from bulk metal and single atom due to their high surface area and quantum size effects.[1] The electronic properties of metal nanoparticles are an important target of condensed matter physics from the viewpoint of quantum size effect and electron confinement effect, and their mesoscopic features make them a key material in nano-device applications. At the same time, chemical modifications of the nanoparticle surfaces are expected to give functionalized supramolecular systems. In recent decades, under such impetus, various kinds of methods have been reported on synthesizing nanoscale metal particles.[2−6] Meanwhile, from a supramolecular chemistry aspect, the majority of research studies have focused on studying properties of the metal nanoparticles covered by different coating layers,[7] where many small molecular ligands, surfactants, and polymers have been used to coat metal nanoparticles. Here, the coating layer can not only control the size of the nanoparticles, but also affect the chemical and physical properties of the nanoparticles. However, the effects of the coating layer on the electronic structure of nanoparticles have not been well recognized as a target of investigations, although they play an essential role in characterizing their electronic features, which are entirely different from those of naked nanoparticles. In some cases, the difference in the properties derives from either the change of exterior surroundings or structure change of the particle surface. Moreover, the interface between the molecules in the coating layer and the atoms of the interior nanoparticle is expected to produce features different from both ingredients, when chemical bonding is generated at the interface. Therefore, investigation of properties generated at the nanoparticle/coating layer interface is of particular interests in supramolecular chemistry and nanoscopic physics.

Among coating materials, alkanethiol is known to be a good stabilizer for metal nanoparticles. Brust et al.[8] brought forward the synthesis of alkanethiol-stabilized metal nanoparticles, opening a new field of self-assembled monolayers. Yee et al.[9] developed a one-phase synthesis method, which provided a convenient way to synthesize thiol-functionalized platinum nanoparticles. In these systems, it is expected that the formation of a sulfur−metal atom bond gives unconventional electronic features at the interface.

In the present paper, octadecanethiol-coated platinum nanoparticles are characterized by transmission electron microscopy, X-ray diffraction, X-ray photoelectron spectroscopy, electron spin resonance, and magnetic susceptibility in order to clarify the structure and the electronic properties generated at the interface between metal nanoparticle and coating layer. The variation of properties caused by the different coverage of the coating layer is discussed.

Experimental Section

Synthesis of the Pt nanoparticles was carried out according to the literature method.[9] The typical process is as follows: dihydrogen hexachloroplatinate(IV) hexahydrate ($H_2PtCl_6 \cdot 6H_2O$) 0.259 g and octadecanethiol ($C_{18}H_{37}SH$) 0.143 g were dissolved in 10 mL of THF freshly distilled from sodium/benzophenone ketyl prior to use, and then a solution of lithium triethylborohydride in THF (1.0 M, 10 mL) was added. The color of the mixture turned from bright yellow to dark brown immediately. After stirring for 40 min, the resulting solution gave colloidal Pt nanoparticles. The nanoparticles were precipitated by adding anhydrous ethanol and were washed several times to remove all starting materials. Finally, the nanoparticles were dried under vacuum condition. The nanoparticles powder can be redissolved in THF. By changing the amount of octadecanethiol in the synthesis, Pt nanoparticles covered with different amounts of organic layer were obtained. Elemental analysis was carried out to estimate the molar ratio of octadecanethiol to Pt. Transmission electron microscopy (TEM) photographs were taken by using a JEOL FE-TEM JEM-2010F instrument with an acceleration voltage of 200 kV. Specimens were prepared by dropping the redissolved nanoparticles solution in THF upon a copper grid covered with a perforated carbon

* Corresponding author. Telephone and Fax: 81-(0)3-5734-2242. E-mail: tenoki@chem.titech.ac.jp.

10.1021/jp034738p CCC: $25.00
Published on Web 08/26/2003

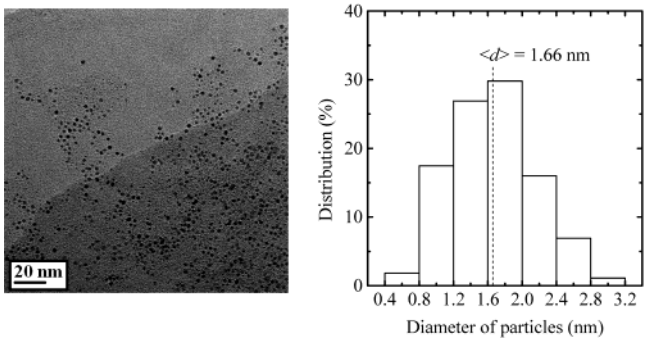

Figure 1. TEM photograph and size distribution histogram of the Pt-0.52 nanparticles. The average diameter is denoted as $\langle d \rangle$.

film and then evaporating the solvent at room temperature. The average diameter of the particles was determined from diameters of 300 nanoparticles found in an arbitrarily chosen area in the TEM photographs. The X-ray diffraction (XRD) pattern was recorded by Rigaku RINT 2000 diffractometer with a Cu rotating target. X-ray photoelectron spectroscopy (XPS) measurements were carried out on an X-ray photoelectron spectrometer Phi5500 MT (ESCA/MC/SAM) with an Mg Kα X-ray source. The Pt nanoparticles powder was put on an indium film. All binding energy values were referred to carbon ($C_{1s} = 285.0$ eV). The magnetic susceptibility and magnetization of the Pt nanoparticles powder were measured with a Quantum Design MPMS-5 DC-SQUID magnetometer in the temperature range 2−300 K under magnetic fields up to 5.5 T. Electron spin resonance (ESR) spectra were measured in the temperature range down to 5 K with an X-band spectrometer (JEOL JES-TE200) equipped with a continuous-flow He cryostat (Oxford ESR 910), where the magnetic field and microwave frequency were calibrated using a NMR field meter and a frequency counter, respectively.

Results

Octadecanethiol-coated Pt nanoparticles were synthesized with a chemical reduction method in one organic phase. By varying the amount of octadecanethiol in the reaction system, Pt nanoparticles covered with different amounts of octadecanethiol layer were synthesized. Pt nanoparticles with four compositions were obtained. These nanoparticles are denoted as $(C_{18}H_{37}SH)_n$Pt, where n is the molar ratio of the coating organic compound to the platinum. According to the values n determined from element analysis, the sample names are abbreviated as Pt-0.31, Pt-0.52, Pt-0.99, Pt-1.05, where the numbers represent n.

A TEM photograph and a size distribution histogram of the Pt-0.52 nanoparticles are shown in Figure 1 as a representative of all the samples. Other samples have similar particle shapes and size distributions. These Pt nanoparticles have spherical shape with a uniform diameter. Average diameters $\langle d \rangle$ are estimated as 1.78, 1.66, 1.15, and 0.93 nm for Pt-0.31, Pt-0.52, Pt-0.99, and Pt-1.05 particles, respectively. It is revealed that the Pt nanoparticles have smaller size with a larger amount of organic coating layer, as summarized in Figure 2a. Formation of the Pt nanoparticles includes two steps: the first one is the reduction of metal precursor $H_2PtCl_6 \cdot 6H_2O$ to metal atoms, and the second one is the growth of nanoparticles from metal atoms. The growth of the Pt nanoparticles can be inhibited by the interaction between the organic molecules and surface atoms of the Pt particles, which causes particles to separate from each other. When a larger amount of organic coating molecules exist in the reaction system, the coverage of the alkanethiol on the

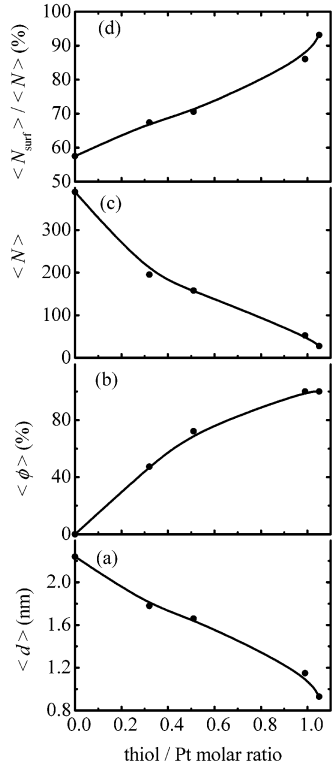

Figure 2. The thiol/Pt ratio dependence of the particle diameter $\langle d \rangle$ (a), the surface coverage $\langle \phi \rangle$ (b), the average number of Pt atoms $\langle N \rangle$ involved in a particle (c), and the percentage of surface Pt atoms $\langle N_{surf} \rangle / \langle N \rangle$ (d). All the data for the naked Pt particle (thiol/Pt = 0) is obtained from ref 11. Solid lines are the guides for the eyes.

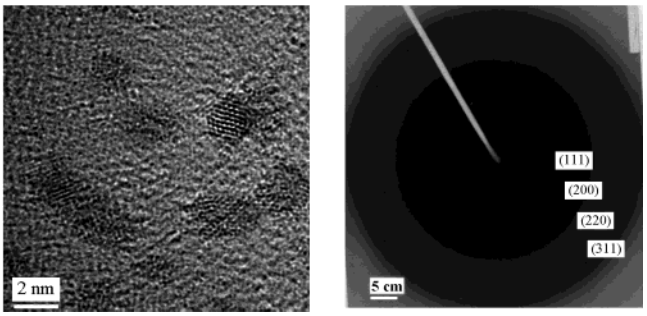

Figure 3. High-resolution TEM photograph (a) and diffraction pattern with Pt diffractions (111), (200), (220) and (311) (b) for the Pt-0.52 nanoparticles.

Pt particles is higher, resulting in smaller sizes of the nanoparticles and better stability of the colloidal particles. In Figure 3, the high-resolution TEM image shows the lattice picture of the particles, proving that the individual nanoparticle forms single crystals with high regularity. The electron diffraction of the Pt-0.52 nanoparticles in Figure 3 shows a face-centered cubic (fcc) packing arrangement with a lattice constant of $d_{(111)} = 0.227$ nm, which is the same as that of bulk Pt. Other samples have similar structure features from TEM observations.

Figure 4 presents the XRD spectrum of the Pt-0.52 particles. The Pt diffraction peaks of (111), (200), (220), and (311) are obviously observed, providing that the Pt nanoparticles have a fcc crystal structure, consistent with the TEM results. According to the Debye−Scherrer formula, the average size of Pt particles calculated from the half width of the diffraction peak (111) is ∼1.7 nm, which is in good agreement with the TEM results. For Pt-0.99 and Pt-1.05 particles, only a dispersed peak of (111) can be obtained in the XRD pattern because of their small particle sizes.

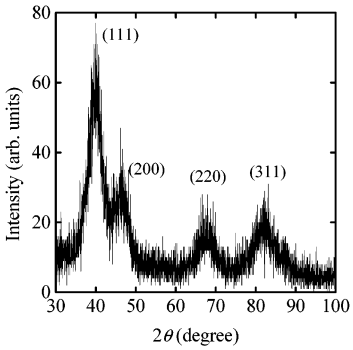

Figure 4. XRD spectrum of the Pt-0.52 nanoparticles with the Pt diffraction indices.

Figures 2a and 2b summarize the thiol/Pt molar ratio dependence of particle diameter $\langle d \rangle$ and surface coverage $\langle \phi \rangle$ with octadecanethiol molecules, respectively. Figures 2c and 2d give the average number $\langle N \rangle$ of Pt atoms involved in a particle and the percentage of surface Pt atoms $\langle N_{surf} \rangle / \langle N \rangle$. With an assumption that particles have spherical shape, $\langle N \rangle$ and $\langle N_{surf} \rangle$ are calculated from the average diameter $\langle d \rangle$ as follows:

$$\langle N \rangle = \frac{{}^4/_3\pi(\langle d \rangle/2)^3}{{a_0}^3/4} \quad (1)$$

$$\langle N_{surf} \rangle = \frac{{}^4/_3\pi((\langle d \rangle/2)^3 - ((\langle d \rangle - \sqrt{2}a_0)/2)^3)}{{a_0}^3/4} \quad (2)$$

where a_0 is the constant of crystal unit with 0.3923 nm. The surface coverage increases monotonically as the thiol/Pt molar ratio is elevated, and it becomes saturated around the ratio of unity, where almost all surface Pt atoms are bonded to sulfur atoms of thiol molecules. The total number of Pt atoms is lowered from ca. 400 to ca. 30 upon the increase in the thiol/Pt molar ratio from 0 to ~1. In contrast, the percentage of surface Pt atoms increases from 57% to 93%.

In a previous report by Yee et al.,[9] stable colloidal Pt nanoparticles coated with an octadecanethiol layer, prepared following the one-phase method, have an average size of ~3 nm. On the other hand, the Pt nanoparticles we synthesized have smaller sizes (less than 2 nm), although the synthesis methods are same. As is known, the faster reduction of the metal precursor and thus the faster nucleation of the metal particles will lead to the smaller particle sizes.[10] It is therefore supposed that the rate of addition of the reducing agent may be somewhat faster in the present case, which will accelerated the reduction of metal precursor and the particle nucleation, giving the smaller particle sizes.

Magnetic susceptibility of the Pt nanoparticles was measured at 2−300 K under 1 T. The susceptibility χ of all the samples obeys the Curie law in the whole temperature range observed, as expressed by $\chi = C/T + \chi_0$, where C and χ_0 are the Curie constant and the temperature-independent term of the susceptibility, respectively. Due to the core diamagnetic susceptibility of the coating organic compound, the constant susceptibility χ_0 is negative for all the particles. By subtracting this contribution of the organic component, the temperature-independent susceptibility for the interior Pt nanoparticles can be calculated. Figures 5a and 5b give the particle diameter dependence of the temperature-independent susceptibility per gram ($\chi_{0g}{}^{Pt}$) and per particle ($\chi_0{}^{Pt}$), respectively, where the estimated $\chi_{0g}{}^{Pt}$ is much smaller than that of bulk Pt (0.983×10^{-6} emu/g). It can be seen that $\chi_{0g}{}^{Pt}$ decreases as the particle diameter becomes small. It should be noted that $\chi_0{}^{Pt}$ corresponds to the Pauli susceptibility at temperature high enough in comparison with the energy discreteness. The spin concentration per gram (n_s) and per particle (N_s) are shown in Figures 6a and 6b, respectively, which are estimated from the Curie constant C with an assumption of $s = 1/2$ and $g \sim 2$. The value n_s shows a dramatic enhancement at higher thiol/Pt ratio, compared with the naked Pt nanoparticles.[11] The spin concentration per particle (N_s) is negligibly small (~0.04 spin per particle) for the naked nanoparticles having an average diameter of 2.2 nm, which is consistent with the particles of the even-electron system for Pt, where the presence of spins is considered to be associated mainly with the spin−orbit interaction effect.[1a] In contrast, for the octadecanethiol-coated Pt nanoparticles, N_s is around 0.3−0.6 spin per particle, more than 1 order of magnitude larger than that for the naked Pt particles. In addition, N_s is insensitive to the particle diameter and the thiol/Pt ratio in the octadecanethiol-coated particles. These experimental findings indicate that the number of spins depends on whether particles are covered by the thiol-monolayers or not. Moreover, it is deduced that each particle has 1 or 0 spin, judging from the spin concentration N_s observed and taking into account that particles having odd and even electrons should have 1 or 0 spin, respectively, although the spin−orbit interaction modifies the spin states.[1a]

Figure 7 shows the magnetization curves of the Pt nanoparticles at 2 K accompanied by Brillouin curves. The observed

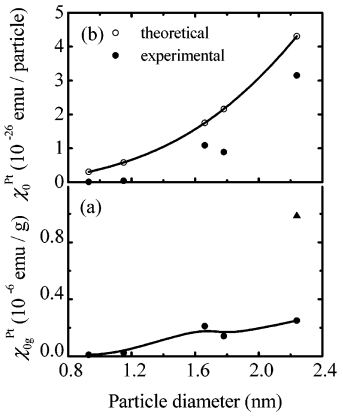

Figure 5. The particle diameter dependence of the temperature-independent susceptibility $\chi_{0g}{}^{Pt}$ per gram (a) and $\chi_0{}^{Pt}$ per particle (b) for the Pt nanoparticles. A triangular symbol refers to the value for bulk Pt. Theoretical values for $\chi_0{}^{Pt}$ are also plotted (see text). Solid lines are the guides for the eyes.

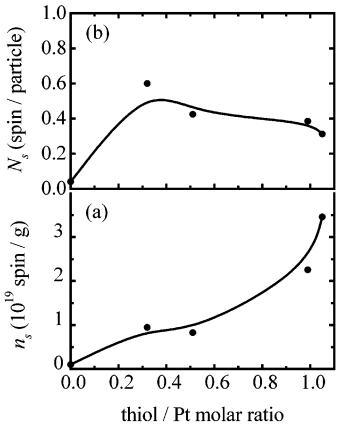

Figure 6. The thiol/Pt ratio dependence of the spin concentration n_s per gram (a) and N_s per particle (b). Solid lines are the guides for the eyes.

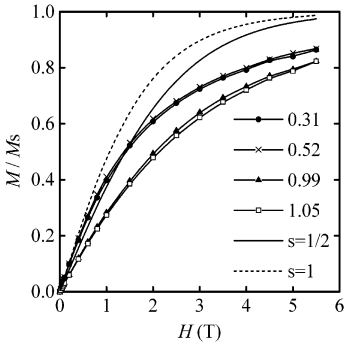

Figure 7. The magnetization curves of the Pt nanoparticles at 2 K, where M_s is the saturation value. The Brillouin curves with $s = 1/2$ and 1 are also depicted with solid and dashed lines, respectively.

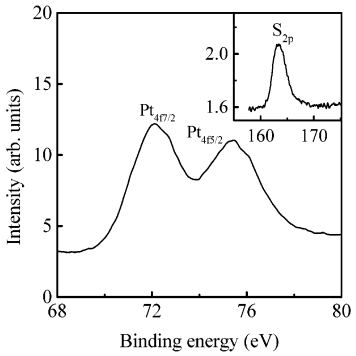

Figure 8. XPS spectra of the Pt-0.99 nanoparticles with Pt_{4f} and S_{2p} binding energies.

magnetization curves show less saturated behavior in comparison with the Brillouin curves with $s = 1/2$ and $s = 1$. This less-saturated feature in the magnetization curves is pronounced in the particles having the higher amount of the coating layer or smaller particle diameter. Taking into account the absence of exchange interaction evidenced by the temperature dependence of the magnetic susceptibility and the linear field dependence of the magnetization in conduction electrons, the less saturated behavior indicates that the nanoparticles have an intermediate state between localized and delocalized electron states, which infer the mobile electrons existing in the Pt particles.

XPS gives an important clue in characterizing the electronic state of the metal particles. The XPS spectra of the Pt-1.05 particles are shown in Figure 8. The binding energy (BE) scales are referenced by setting the C_{1s} BE to 285.0 eV, referring to the value observed in refs 12 and 13. The BEs of $Pt_{4f7/2}$ and $Pt_{4f5/2}$ are 72.0 and 75.3 eV, respectively, which shift to high binding energies compared with those of bulk Pt ($Pt_{4f7/2}$, 71.2 eV; $Pt_{4f5/2}$, 74.5 eV).[14] In contrast, the BE of S_{2p} for the octadecanethiol molecules coating Pt particles is 163.2 eV, which shifts to lower binding energy than the pure octadecanethiol molecules (163.8 eV).[12] These results are consistent with a previous study by Fu et al.,[13] who measured the Pt_{4f} peak shift of Pt nanoparticles covered with several modified layers and concluded the thiol-bonding effect.

ESR spectra measured at room temperature show Lorentzian line shape for all the samples. Figure 9 shows the thiol/Pt ratio dependence of the squared g-value deviation Δg^2 ($= (g - g_0)^2$) and the line width ΔH, where g_0 with the g-value of free electron spin is 2.0023. The similar tendency between Δg^2 and ΔH in the dependence on the amount of organic layer is suggestive of the importance of the spin−lattice relaxation in the electron spins. It is clearly seen that Δg^2 and ΔH rise dramatically with an increasing amount of the coating thiol layer on the particles.

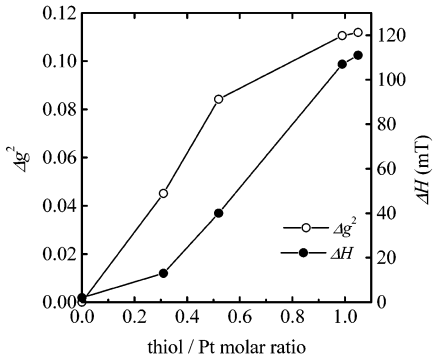

Figure 9. The thiol/Pt ratio dependence of Δg^2 and ΔH measured at room temperature for the thiol-coated Pt nanoparticles. The data for the naked Pt particle (thiol/Pt = 0) is obtained from ref 15.

Indeed, for the Pt-1.05 nanoparticles with full coverage, Δg and ΔH are very large, with the value of 0.335 and 111 mT, respectively, which are contrasted with 0.0004 and 2 mT for the naked Pt nanoparticles,[15] suggesting orders-of-magnitude increases. The large Δg and ΔH values indicate the generation of the fast spin−lattice relaxation centers in the octadecanethiol-monolayer-coated Pt particles. These findings prove that the coating organic layer plays an important role in the features of the ESR signals. The g-value and the line width are found to be independent of the temperature.

Discussion

In characterizing the electronic properties of a nanosized particle, quantum size effect is one of the most important issues.[16,17] The discreteness δ in the energy levels becomes comparable to the thermal energy when the size of the system becomes in the nanometer dimension. Spin susceptibility is typically reflected by the quantum size effect. The spin susceptibility, which is independent of temperature as the Pauli susceptibility in bulk metal, is modified as expressed by the following equation:[16]

$$\chi_0 = 2\mu_B{}^2/\delta \qquad (3)$$

in the high-temperature limit. When the temperature is lowered to the range comparable to or below δ, the susceptibility tends to go zero or gives Curie-type divergence for systems having even or odd numbers of electrons, respectively, though the spin−orbit interaction modifies this feature.[1a,17] Therefore, a Pt particle, which is featured by an even-electron system when it is neutral, should obey eq 3 at high temperatures and becomes zero as the temperature goes to zero. The observed susceptibility showing Curie's behavior is somewhat different from that expected at low temperatures. Especially, the deviation is clear when we compare the behaviors between the thiol-coated and naked nanoparticles, as mentioned before.

Here, we discuss the correlation between the energy discreteness and the susceptibility. The size dependence of the energy discreteness is represented by the following equation; $\delta \sim E_F/N$ with the Fermi energy E_F and the number of Pt atoms N involved in a particle. According to the result calculated with the equation and $E_F \sim 9.71$ eV,[18] the estimated δ increases from 0.025 to 0.35 eV as the particle size is lowered from 2.2 to 0.9 nm. The susceptibilities at infinite temperature, which correspond to $\chi_0{}^{Pt}$ obtained in the experiments and theoretical calculation with eq 3, are plotted in Figure 5b. The susceptibility estimated from δ semiquantitatively represents the experimental results with $\chi_0{}^{Pt}$, suggesting an important role of the quantum size effect in the

magnetic properties. The itinerant feature modified by the quantum size effect in the magnetism also appears in the magnetization vs field curves. As shown in Figure 7, the magnetizations experimentally obtained have less saturated behavior in comparison with the Brillouin curves with $s = 1/2$ or 1. They are also far from a linear magnetization vs field relation expected in bulk Pauli paramagnetism. Eventually, it is considered that the weak convex curvature in the magnetization curve is associated with the presence of energy discreteness, giving a trace of localized electronic features.[16]

The susceptibility showing a Curie-type divergence at low temperatures is apparently in disagreement with that expected for the even-electron system. The spin concentration estimated from the Curie's contribution is in the range of 0.3−0.6 spin/particle, where the spin concentration is regarded as the mean spin concentration in all the particles involved with the particle diameter distribution presented in Figure 1. This means that individual particles have less than 1 spin, or, in other words, one or zero spin exists in a particle. Consistency between the experimental observation and the theoretical prediction is obtained by taking into account the modification of the electronic state at the interface between the interior Pt particle and surface-covering thiol molecules, as we can see in the XPS spectra.

The XPS spectra of the Pt nanoparticles show that Pt_{4f} peaks shift to higher binding energy by 0.8 eV compared with bulk Pt. Two major reasons can be considered for the peak shift of metal nanoparticles separated from the substrate by modified layer. One arises from a unit positive charge remaining on a nanoparticle in the photoemission final state.[19] Unless the substrate is not conducting enough, there will remain an excess unit positive charge distributed over the surface of a nanoparticle during the time scale of photoelectron emission and the charge results in Coulomb attraction that increases the apparent binding energy. This is the Coulomb blockade effect and the energy difference can be expressed as $\Delta E = e^2/2C$, where C is the self-capacitance of the nanoparticle. ΔE increases as the particle size decreases because of the decrease in C. Recently, the core-level peak shift of Au nanoparticles supported on an octanedithiol self-assembled monolayer (SAM) on Au(111) was explained in terms of the Coulomb blockade effect in combination with scanning tunneling spectroscopy (STS) measurements.[20] The other reason for the peak shift comes from bonding and charge transfer between the metal particle and the modified layer. Fu et al.[13] compared the Pt_{4f} peak shift of Pt nanoparticles that had an average particle core diameter of 1.3 nm and were covered with different modified layers. They conclude that there is a contribution of the ligand effect for the Pt particles covered by $C_{12}H_{25}SH$ because the peak shift is higher than that in other ligands having weaker interaction with the Pt core by 0.3 eV in addition to the presence of a negative shift of −0.6 eV for the S_{2p} peak compared with free $C_{12}H_{25}SH$. The peak shifts observed in the present study are −0.6 eV for the S_{2p} and +0.8 eV for the Pt_{4f} in comparison with free octadecanethiol and bulk Pt, respectively. These values are quite consistent with those obtained by Fu et al.,[13] by considering the smaller core diameter of 0.93 nm for the present case. Therefore we conclude that there is a ligand effect for the Pt_{4f} peak shift originating from the charge transfer from the metal core to the thiol-coating layer. The charge transfer causes electron deficient features in the electronic structure in the interior Pt nanoparticle, which produces the deviation of the interior Pt nanoparticle from an even-electron system, resulting in the generation of Curie's spins.

Here arises a question on the charge transfer effect at the interface; that is, "Can the charge transfer effect be purely extracted from the experimental results independent of the quantum size effect?" To clarify this context, we tried to prepare naked nanoparticles whose sizes were less than 2 nm. The obtained naked particles were rapidly coagulated just after vacuum-drying and subjected to the subsequent oxidation reaction as evidenced by the color change to gray. Such change in the feature of nanoparticles is pronounced as the particle size becomes small. Therefore, from the experimental viewpoint, it is very difficult to separate these two effects. In addition, even in the theoretical stance, both effects are not absolutely independent of each other since the reduction in size changes the surface state. In other words, charge transfer at the interface is also affected to some extent by the change in the particle size. This is consistent with the experimental results showing a deviation from what theory predicts, as shown in the temperature-independent susceptibility in Figure 5. In relation to the correlation between the two effects, the behavior of the localized spin concentration N_s exhibited in Figure 6 is didactic. The difference between the naked nanoparticles and the thiol-coated nanoparticles is clearly seen by comparing between the plotted points at thiol/Pt molar ratios of 0 and 0.31, where the latter corresponds to 47% coverage, suggesting the importance of a charge-transfer effect at the interface for the thiol-coated nanoparticles. In contrast, the experimental finding of the gradual and weak declining of the spin concentration upon the rise of the thiol/Pt molar ratio above 0.31 is considered to come from a trace of size effect, taking into account that the reduction of thiol/Pt molar ratio corresponds to the decrease in the particle size. The ionization potential of the particle is elevated as the particle size becomes small in general, approaching the ionization potential of a single atom at the extreme. This means that charge-transfer becomes more and more difficult upon the decrease in the particle size, resulting in a decrease in the number of nanoparticles having odd number of electrons. Eventually, the slight declining trend in the localized spin concentration is the consequence of the size effect.

The interaction at the interface also importantly contributes to the spin−lattice relaxation mechanism as evidenced by the thiol/Pt molar ratio dependence of the ESR g-value and the line width shown in Figure 9. Compared with the naked Pt nanoparticles,[15] the octadecanthiol-coated Pt nanoparticles have large deviations of g-values and large line widths. Actually, the g-value deviation increases from 0.0004 to 0.3345 as the thiol/Pt ratio is elevated from 0 to 1, while the line width increases from 2 mT to 111mT. The line width at thiol/Pt $\sim$ 1 is indeed 2 orders of magnitude as large as that of the naked Pt nanoparticles. These experimental findings prove that the spin−lattice relaxation rate is considerably accelerated in the octadecanthiol-coated Pt nanoparticles, suggesting that the modification in the electronic structure at the interface works to contribute to the fast spin−lattice relaxation mechanism through the enhancement of spin−orbit interaction.

According to theoretical suggestion,[21,22] the line width ΔH associated with the spin−lattice relaxation and the spin−lattice relaxation time T_1 are expressed by the following equations:

$$\Delta H \approx \frac{\hbar}{2\sqrt{3}g\mu_B T_1} \tag{4}$$

$$\frac{1}{T_1} \approx \alpha(\Delta g)^2\left(\frac{1}{\tau_b} + \frac{1}{\tau_p}\right) \tag{5}$$

where α is a numerical factor whose magnitude is on the order

of 1, and τ_b and τ_p are the scattering times associated with electron-scattering events by particle boundaries and phonons, respectively. The *g*-value deviation is related to the spin−orbit interaction ζ as given by

$$\Delta g \propto \zeta \sum_{n \neq 1} \frac{\langle 0|l|n\rangle\langle n|l|0\rangle}{E_n - E_0} \tag{6}$$

where l, ζ, E_0, and E_n are the orbital angular momentum, the spin−orbit interaction, and the energies of the ground state and the *n*th excited state. The phonon-assisted scattering has temperature dependence in general, since the phonon excitation is thermally activated, whereas the boundary-scattering contribution is temperature-independent. The experimental results indicate that the ESR line width is independent of temperature. The mean free path of an electron subjected to the electron−phonon scattering process is in general in the range of >10 nm.[23] Therefore, the phonon-assisted scattering is not at work in the present nanoparticles since the particle diameter $\langle d \rangle$ is more than 1 order of magnitude as small as the mean free path of the phonon scattering. In other words, the spin−lattice relaxation is governed by the particle boundary scattering, as confirmed by the temperature-independent feature of the line width. The scattering time in the boundary scattering is given as $\tau_b = \langle d \rangle / \nu_F$, where ν_F is the Fermi velocity. Using the observed particle diameter, the *g*-value deviation, and the $\nu_F \sim 1.85 \times 10^6$ m/s (calculated from $E_F = m_e \nu_F^2/2$, where m_e is the mass of an electron) for bulk Pt and $\alpha \approx 1$, T_1 is estimated from eq 5 as 5.6×10^{-15} s and 7.6×10^{-9} s for octadecanthiol-coated 1.0 nm Pt particles and the naked Pt particles, respectively, which are in qualitative agreement with the experimental values of T_1 obtained from eq 4, 1.3×10^{-11} s and 0.82×10^{-9} s for the former and the latter, respectively, although a large deviation exists for the thiol-coated nanoparticles, and especially, the estimated value for the 1.0 nm octadecanethiol-coated Pt particles is unrealistically short. The deviation between the observed and estimated results might be considered to originate from the ambiguity in the Fermi velocity due to the energy discreteness generated in the small diameter particle with $\langle d \rangle \sim 1$ nm, where δ is estimated as ~0.3 eV. In addition, for particles, whose energy discreteness is orders of magnitude larger than the Zeeman energy ($\delta \gg \hbar\omega_z$), the correction for the quantum size effect modifies eq 5 as follows:

$$\frac{1}{T_1} \approx \alpha(\Delta g)^2 \left(\frac{1}{\tau_b} + \frac{1}{\tau_p}\right) \frac{\hbar\omega_z}{\delta} \tag{7}$$

where $\hbar\omega_z$ is the Zeeman energy. Indeed, the present Pt nanoparticles having the sizes in the range of ~1−2 nm are subjected to the quantum correction, since the line width observed is orders of magnitudes as small as that expected with the ordinary size effect with no quantum correction. Calculation from eq 7 gives $T_1 \sim 3.3 \times 10^{-10}$ s for 1.0 nm thiol-coated Pt particles, which is elevated comparing with that estimated without quantum correction and approaches the experimental value of 1.3×10^{-11} s, although the applicability of eq 7 is in question since the interface effect should be taken into account in the estimation of T_1. Eventually, it is confirmed that the presence of fast relaxation sites at the interface work to accelerate the spin−lattice relaxation process in thiol-coated Pt particles.

Hence, the origin of the fast relaxation should be addressed. In this connection, the discontinuous potential change at the interface can contribute to the enhancement in the spin−orbit interaction.[23] In the naked nanoparticle, the Pt atoms face to vacuum at the well-defined surface, where a discontinuity is present in the potential. At the surface, the spin−orbit interaction ζ is enhanced owing to the discontinuous change in the potential V as given by the following equation:

$$\zeta \propto \left\langle \frac{1}{r} \text{grad } V \right\rangle |\psi(r,E_F)|^2 \tag{8}$$

where, $\langle\rangle$ is the time average and $\psi(r,E_F)$ is the wave function at the Fermi energy E_F and the surface. The wave functions of the conduction electrons have a steep decay at the surface. The steep decay of the wave function at the surface makes the potential gradient contribute less to the enhancement in the spin−orbit interaction. In contrast, for thiol-molecule-bonded nanoparticle, the wave function of the Pt conduction electron can penetrate the interfacial region, extended to the covering thiol molecules due to the charge transfer from the interior Pt atoms to the thiol molecules. The large conduction electron density at the interface effectively enhances the spin−orbit interaction. Therefore, the enhanced spin−orbit interaction gives the fast relaxation centers at the interface. Here, it should be noted that the contribution of an alkyl chain to the interface electronic state is absent. The energy levels of S atom origin (3*s*, 3*p*) are closed to the Fermi energy of Pt nanoparticles.[24] The wave function hybridized between S and Pt is present around E_F. However, the σ levels of alkyl chains located far from the Fermi energy can give only a negligible contribution to the interface electronic state.

Summary

Pt nanoparticles coated with different amounts of octadecanethiol molecules are synthesized. Their average particle sizes vary from 1.8 to 0.9 nm, accompanied with the increasing coverage of nanoparticle surface from 50% to full coverage by thiol molecules. They show unconventional properties that differ from the case of naked Pt nanoparticles. The spin susceptibility of all these thiol-coated Pt particles, which is smaller than that of bulk Pt, rises upon the increase in the particle size, thus quantum size effect being suggested to govern the magnetism. XPS spectra suggest the electron deficiency for Pt atoms in the particles, which derives from charge transfer from Pt nanoparticle to the coating thiol layer. The electron deficiency thus produced causes the electronic structure of Pt to deviate from the even-electron state, which causes the enhanced Curie's behavior of the susceptibility at low temperatures. ESR line width and the *g*-value shift of the thiol-coated particles become dramatically larger than those of naked ones upon the increase in the thiol/Pt ratio, which are associated with the enhancement of spin−orbit interaction at the interface between the interior Pt nanoparticle and the coating thiol monolayer. The discontinuous potential change and charge transfer at the interface can contribute to the enhancement in the spin−orbit interaction. This change at the interface gives rise to the first spin−lattice relaxation centers in the carrier scattering process.

Acknowledgment. The authors express their sincere thanks to Prof. S. Bandow, Prof. K. Kimura, and Prof. K. Sugihara for fruitful discussion. The present work was partly supported by a Grant-in-Aid for Scientific Research on Priority Area (No. 12046231). W.T. was supported by the Japan Science Promotion Society Postdoctoral Fellowship for Foreign Researchers.

References and Notes

(1) (a) Halperin, W. P. *Rev. Mod. Phys.* **1986**, *58*, 533. (b) Thomas, J. M. *Pure Appl. Chem.* **1988**, *60*, 1517. (c) Schmid, G. *Clusters and Colloids*;

VCH: Weinheim, 1994. (d) Schmid, G. *Chem. Rev.* **1992**, *92*, 1709. (e) Gates, B. C. *Chem. Rev.* **1995**, *95*, 511. (f) Volokitin, Y.; Sinzig, J.; de Jong, L. J.; Schmid, G.; Vargaftik, M. N.; Moiseev, I. I. *Nature* **1996**, *384*, 621. (g) Sugano, S. *Microcluster Physics*; Springer-Verlag: Berlin, 1991.

(2) Hirai, H. *J. Macromol. Sci., Chem.* **1979**, *A13*, 633.

(3) Torigoe K.; Esumi, K. *Langmuir* **1993**, *9*, 1664.

(4) (a) Esumi, K.; Tano T.; Meguro, K. *Langmuir* **1989**, *5*, 268. (b) Bradley, J. S.; Hill, E. W.; Klein, C.; Chaudret, B.; Duteil, A. *Chem. Mater.* **1993**, *5*, 254.

(5) (a) Bowles, R. S.; Kolstad, J. J.; Calo, J. M.; Andres, R. P. *Surf. Sci.* **1981**, *106*, 117. (b) Klabunde, K. J.; Li Y. X.; Tan, B. J. *Chem. Mater.* **1991**, *3*, 30.

(6) Suslick, K. S.; Choe, S. B.; Cichowlas, A. A.; Grinstaff, M. W. *Nature* **1991**, *353*, 414.

(7) (a) Golden, J. H.; Deng, H.; Disalvo, F. J.; Fréchet, J. M. J.; Thompson, P. M. *Science* **1995**, *268*, 1463. (b) Watkins, J. J.; McCarthy, T. J. *Chem. Mater.* **1995**, *7*, 1991. (c) Chan, Y.; Ng, C.; Craig, G. S. W.; Schrock, R. R.; Cohen, R. E. *Chem. Mater.* **1992**, *4*, 885. (d) Tu, W.; Liu, H.; Liew, K. Y. *J. Colloid Interface Sci.* **2000**, *229*, 453.

(8) (a) Brust, M.; Walker, M.; Bethell, D.; Schiffrin, D. J.; Whyman, R. *J. Chem. Soc., Chem. Commun.* **1994**, 801. (b) Brust, M.; Fink, J.; Bethell, D.; Schiffrin, D. J.; Kiely, C. J. *J. Chem. Soc., Chem. Commun.* **1995**, 1655.

(9) (a) Yee, C.; Jordan, R.; Ulman, A.; White, H.; King, A.; Rafailovich, M.; Sokolov, J. *Langmuir* **1999**, *15*, 3486. (b) Yee, C.; Scotti, M.; Ulman, A.; White, H.; Rafailovich, M.; Sokolov, J. *Langmuir* **1999**, *15*, 4314.

(10) Tu, W.; Liu, H. *J. Mater. Chem.* **2000,** *10*, 2207.

(11) Marzke, R. F.; Glaunsinger, W. S.; Bayard, M. *Solid State Commun.* **1976**, *18*, 1025.

(12) Castner, D. G.; Hinds, K.; Grainger, D. W. *Langmuir* **1996**, *12*, 5083.

(13) Fu, X.; Wang, Y.; Wu, N.; Gui, L.; Tang, Y. *J. Colloid Interface Sci.* **2001**, *243*, 326.

(14) Briggs, D., Seah, M. P., Eds.; *Practical Surface Analysis, Vol. 1, Auger and X-ray Photoelectron Spectroscopy*; Wiley: Chichester, 1990.

(15) Gordon, D. A.; Marzke, R. F.; Glaunsinger, W. S. *J. Phy.* **1977**, *38*, C2−87.

(16) Kubo, R. *J. Phys. Soc. Jpn.* **1962**, *17*, 952.

(17) Denton, R.; Mühlschlegel, B.; Scalapino, D. J. *Phys. Rev. B* **1973**, *7*, 3589.

(18) Krogh Andersen, O.; Mackintosh, A. R. *Solid State Commun.* **1968**, *6*, 285.

(19) Wertheim, G. K.; DiCenzo, S. B.; Youngquist, S. E. *Phys. Rev. Lett.* **1983**, *51*, 2310.

(20) Ohgi, T.; Fujita, D. *Phys. Rev. B* **2002**, *66*, 115410.

(21) Elliott, R. J. *Phys. Rev.* **1954**, *96*, 266.

(22) Andersson, O. E.; Prasad, B. L. V.; Sato, H.; Enoki, T.; Hishiyama, Y.; Kaburagi, Y.; Yoshikawa, M.; Bandow, S. *Phys. Rev. B* **1998**, *58*, 16387.

(23) (a) Kawabata, A.; Kubo, R. *J. Phys. Soc. Jpn.* **1966**, *21*, 1765. (b) Kawabata, A. *J. Phys. Soc. Jpn.* **1970**, *29*, 902.

(24) Springbrog, M. *Chem. Phys.* **1999**, *246*, 347.